Research Results of Plasma Focus Numerical Experiments

S LEE[1,2,3] and S H SAW[2,4]
[1]*Institute for Plasma Focus Studies, 32 Oakpark Drive, Chadstone, VIC 3148, Australia*
[2]*INTI University College, 71800 Nilai, Malaysia*
[3]*Nanyang Technology University, National Institute of Education, Singapore 637616*
[4]*University of Malaya, Kuala Lumpur, Malaysia*

e-mail: leesing@optusnet.com.au

Abstract

The Lee model couples the electrical circuit with plasma focus dynamics, thermodynamics, and radiation. A phenomenological beam-target neutron generating mechanism is included in the code to provide information on the neutron yield. The Lee model is extensively used to design and simulate experiments. This paper provides an overview of recent published results from numerical experiments carried out using the Lee model. The results are: (1) a previously unsuspected "pinch current limitation" effect; (2) the existence of an optimum L_o below which the pinch current and neutron yield of that plasma focus would not increase, but instead decreases; (3) a realistic neutron yield scaling with pinch current; and (4) an innovative tool to obtain the pinch current. A dominant thread running through the research papers is that the pinch current has to be distinguished from the discharge peak current in the analysis and scaling of plasma focus experiments.

1. Introduction

The Lee model in its two-phase form was described in 1984 [1]. It was used to assist in the design and interpretation of several experiments [2–4]. An improved five-phase model and code incorporating finite small disturbance speed [5] and radiation coupling with dynamics assisted several projects [6–8] and was web published [9] in 2000 and in 2005 [10]. Plasma self-absorption was included [9] in 2007. It has been used extensively as a complementary facility in several machines, for example, UNU/ICTP PFF [2,6], NX2 [7,8], NX1 [7] and DENA [11]. It has also been used [12] in other machines for design and interpretation including Soto's sub-kilojoule plasma focus machines [13] FNII [14] and the UBA hard x-ray source [15]. Information obtained from the model includes axial and radial velocities and dynamics [1,7,11,12], soft x-ray (SXR) emission characteristics and yield [6-8,16], design of machines [13,16], optimization of machines, and adaptation to other machine types such as the Filippov-type DENA [11]. A study of speed-enhanced neutron yield [17] was also assisted by the Lee model code.

A detailed description of the Lee model is already available on the internet [9,10]. A recent development in the code is the inclusion of neutron yield using a phenomenological beam-target neutron generating mechanism [18] incorporated in the present RADPFV5.13 [19]. This improved model has been used to discover the pinch limitation effect [20], the existence of an optimum L_o below which the pinch current and neutron yield of that plasma focus would not increase, but instead decreases [21], a realistic neutron yield scaling with pinch current [22] and has been proven to be an innovative tool to obtain the pinch current [23].

2. The numerical experiments

Numerical experiments were carried out on plasma focus machines for which reliable current traces and neutron yields are available. The experiment was applied to several machines including the PF400, UNU/ICTP PFF, the NX2 and Poseidon. The PF1000 which has a current curve published at 27kV and Y_n published at 35kV provided an important point.

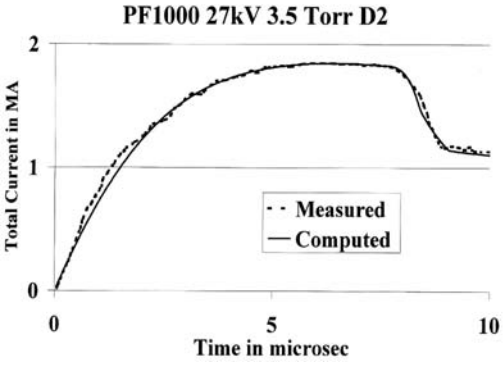

Figure 1. PF1000 at 27kV measured (dashed line) vs computed (smooth line) current traces.

Figure 1 shows a comparison of the computed total current trace (solid smooth line) with the experimental trace (dotted line) of the PF1000 at 27 kV and 3.5 Torr deuterium, with outer/inner radii b=16 cm, a=11.55 cm, and anode length z_o=60 cm. In the numerical experiments we fitted external or static inductance L_o=33 nH and stray resistance r_o=6 mΩ with model parameters mass factor, current factor, and radial mass factor as f_m=0.14, f_c=0.7, and f_{mr}=0.35. The computed current trace agrees very well with the experiment, a typical performance of this code.

Each numerical experiment is considered satisfactory when the computed current trace matches the experiment in current rise profile and peak current, in time position of the current dip, in slope, and absolute value of the dip (see Figure 1). Once this fitting is done our experience is that the other computed properties including dynamics, energy distributions and radiation are all realistic.

3. Pinch current limitation effect

In a recent paper [18] there was expectation that the large MJ plasma focus PF1000 in Warsaw could increase its discharge current, and its pinch current, and consequently neutron yield by a reduction of its external inductance L_o. To investigate this point experiments were carried out using the Lee model code [19]. Unexpectedly, the results indicated that whilst I_{peak} indeed progressively increased with reduction in L_o, no improvement may be achieved due to a pinch current limitation effect [20, 21]. Given a fixed C_o powering a plasma focus, there exists an optimum L_o for maximum I_{pinch}. Reducing L_o further will increase neither I_{pinch} nor Y_n.

We carried out numerical experiments for PF1000 using the machine and model parameters determined from Figure 1, modified by information about values of I_{peak} at 35 kV. Operating the PF1000 at 35 kV and 3.5 Torr, we varied the anode radius a with corresponding adjustment to b to maintain a constant c=b/a in order to keep the peak axial speed at 10 cm/μs. The anode length z_o was also adjusted to maximize I_{pinch} as L_o was decreased from 100 nH progressively to 5 nH.

As expected, I_{peak} increased progressively from 1.66 to 4.4 MA. As L_o was reduced from 100 to 35 nH, I_{pinch} also increased, from 0.96 to 1.05 MA. However, then unexpectedly, on further reduction from 35 to 5 nH, I_{pinch} stopped increasing, instead decreasing slightly to 1.03 MA at 20 nH, to 1.0 MA at 10 nH, and to 0.97 MA at 5 nH. Y_n also had a maximum value of 3.2×10^{11} at 35 nH.

To explain this unexpected result, we examine the energy distribution in the system at the end of the axial phase (see Figure 1) just before the current drops from peak value I_{peak} and then again near the bottom of the almost linear drop to the pinch phase. The energy equation describing this current drop is written as follows:

$$0.5 I_{peak}^2 (L_o + L_a f_c^2) = 0.5 I_{pinch}^2 (L_o / f_c^2 + L_a + L_p) + \delta_{cap} + \delta_{plasma} \quad (1)$$

where L_a is the inductance of the tube at full axial length z_o, δ_{plasma} is the energy imparted to the plasma as the current sheet moves to the pinch position and is the integral of $0.5(dL/dt)I^2$. We approximate this as $0.5 L_p I_{pinch}^2$ which is an underestimate for this case. δ_{cap} is the energy flow into or out of the capacitor during this period of current drop. If the duration of the radial phase is short compared to the capacitor time constant, the capacitor is effectively decoupled and δ_{cap} may be put as zero. From this consideration we obtain

$$I_{pinch}^2 = I_{peak}^2 (L_o + 0.5 L_a) / (2L_o + L_a + 2L_p) \quad (2)$$

where we have taken f_c=0.7 and approximated f_c^2 as 0.5.

Generally, as L_o is reduced, I_{peak} increases; a is necessarily increased leading [17] to a longer pinch length z_p, hence a bigger L_p. Lowering L_o also results in a shorter rise time, hence a necessary decrease in z_o, reducing L_a. Thus, from Eq. (2), lowering L_o decreases the fraction I_{pinch}/I_{peak}. Secondly, this situation is compounded by another mechanism. As L_o is reduced, the L-C interaction time of the capacitor bank reduces while the duration of the current drop increases (see Fig 2, discussed in the next section) due to an increasing a. This means that as L_o is reduced, the capacitor bank is more and more coupled to the inductive energy transfer processes with the accompanying induced large voltages that arise from the radial compression. Looking again at the derivation of Eq. (2) from Eq. (1) a nonzero δ_{cap}, in this case, of positive value, will act to decrease I_{pinch} further. The lower the L_o the more pronounced is this effect.

Summarizing this discussion, the pinch current limitation is not a simple effect, but is a combination of the two complex effects described above, namely, the interplay of the various inductances involved in the plasma focus processes abetted by the increasing coupling of C_o to the inductive energetic processes, as L_o is reduced.

4. Optimum L_o for maximum pinch current and neutron yield

From the pinch current limitation effect, it is clear that given a fixed C_o powering a plasma focus, there exists an optimum L_o for maximum I_{pinch}. Reducing L_o further will increase neither I_{pinch} nor Y_n. The results of the numerical experiments carried out are presented in Figure 2 and Table 1.

With large L_o = 100 nH it is seen (Figure 2) that the rising current profile is flattened from what its waveform would be if unloaded; and peaks at around 12μs (before its unloaded rise time, not shown, of 18μs) as the current sheet goes into the radial phase. The current drop, less than 25% of peak value, is sharp compared with the current rise profile. At L_o = 30 nH the rising current profile is less flattened, reaching a flat top at around 5μs, staying practically flat for some 2μs before the radial phase current drop to 50% of its peak value in a time which is still short compared with the rise time. With L_o of 5 nH, the rise time is now very short, there is hardly any flat top; as soon as the peak is reached, the current waveform droops significantly. There is a small kink on the current waveform of both the L_o = 5 nH, z_o = 20 cm and the L_o = 5 nH, z_o = 40 cm. This kink corresponds to the start of the radial phase which, because of the large anode radius, starts with a relatively low radial speed, causing a momentary reduction in dynamic loading. Looking at the three types of traces it is seen that for L_o = 100 nH to 30 nH, there is a wide range of z_o that may be chosen so that the radial phase may start at peak or near peak current, although the longer values of z_o tend to give better energy transfers into the radial phase.

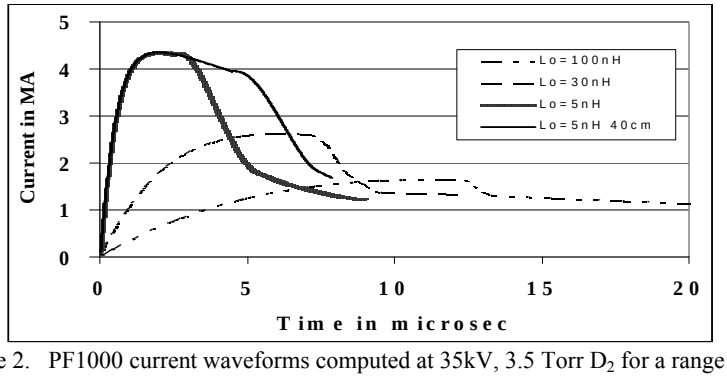

Figure 2. PF1000 current waveforms computed at 35kV, 3.5 Torr D_2 for a range of L_o

The optimized situation for each value of L_o is shown in Table 1. The table shows that as L_o is reduced, I_{peak} rises with each reduction in L_o with no sign of any limitation. However, I_{pinch} reaches a broad maximum of 1.05MA around 40–30 nH. Neutron yield Y_n also shows a similar broad maximum peaking at 3.2×10^{11} neutrons. Figure 3 shows a graphical representation of this I_{pinch} limitation effect. The curve going up to 4MA at low L_o is the I_{peak} curve. Thus I_{peak} shows no sign of limitation as L_o is progressively reduced. However I_{pinch} reaches a broad maximum. From Figure 3 there is a stark and important message. One must distinguish clearly between I_{peak} and I_{pinch}. In general one cannot take I_{peak} to be representative of I_{pinch}.

Table 1. Effect on currents and ratio of currents as L_o is reduced-PF1000 at 35kV, 3.5 Torr D_2

L_0(nH)	b(cm)	a(cm)	z_0(cm)	I_{peak}(MA)	I_{pinch}(MA)	$Y_n(10^{11})$	I_{pinch}/I_{peak}
100	15.0	10.8	80	1.66	0.96	2.44	0.58
80	16.0	11.6	80	1.81	1.00	2.71	0.55
60	18.0	13.0	70	2.02	1.03	3.01	0.51
40	21.5	15.5	55	2.36	1.05	3.20	0.44
35	22.5	16.3	53	2.47	1.05	3.20	0.43
30	23.8	17.2	50	2.61	1.05	3.10	0.40
20	28.0	21.1	32	3.13	1.03	3.00	0.33
10	33.0	23.8	28	3.65	1.00	2.45	0.27
5	40.0	28.8	20	4.37	0.97	2.00	0.22

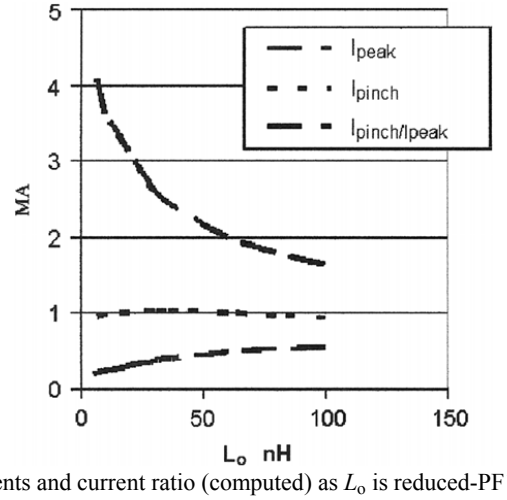

Figure 3. Effect on currents and current ratio (computed) as L_o is reduced-PF1000, 35 kV, 3.5 Torr D_2

We carried out several sets of experiments on the PF1000 for varying L_o, each set with a different damping factor. In every case, an optimum inductance was found around 30–60 nH with I_{pinch} decreasing as L_o was reduced below the optimum value. The results showed that for PF1000, reducing L_o from its present 20–30 nH will increase neither the observed I_{pinch} nor the neutron yield, because of the pinch limitation effect.

5. Neutron yield scaling with pinch current

The main mechanism producing the neutrons is a beam of fast deuteron ions interacting with the hot dense plasma of the focus pinch column. The fast ion beam is produced by diode action in a thin layer close to the anode with plasma disruptions generating the necessary high voltages. This mechanism, described in some details in a recent paper [18], results in the following expression [22] used for the Lee model code:

$$Y_{b\text{-}t} = \textit{calibration constant} \times n_i I_{pinch}^{\,2} z_p^{\,2} (\ln(b/r_p))\sigma / V_{max}^{\,0.5} \qquad (3)$$

where I_{pinch} is the current at the start of the slow compression phase, r_p and z_p are the pinch radius and pinch length at the end of the slow compression phase, V_{max} is the maximum value attained by the inductively induced voltage and σ is the D-D fusion cross section (n branch) [24] corresponding to the beam ion energy. The D-D cross section σ is obtained by using beam energy equal to 3 times V_{max}, to conform to experimental observations [25].

Experimental data [26,27] of neutron yield Y_n against pinch current I_{pinch} is assembled (see Figure 4) to produce a more global scaling law than available. It must be noted that there is no clear distinction shown in the literature of I_{pinch} , I_{peak} and I_{total}. From the data a mid-range point is obtained to calibrate the neutron production mechanism of the Lee model code (Figure 4).

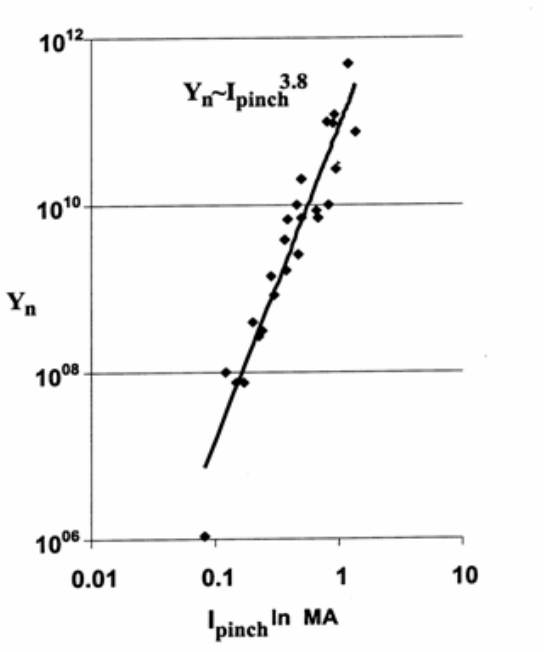

Figure 4. Assembly of experimental data to obtain Y_n scaling with current; loosely termed as the current or pinch current in the literature. This is the experimental curve from which a calibration point is obtained, at 0.5 MA, to calibrate the neutron yield equation (3) for the Lee model code.

We then apply the calibrated code to several machines including the PF400, UNU/ICTP PFF, the NX2 and Poseidon to derive neutron scaling laws from computation. The PF1000 which has a current curve published at 27kV and Y_n published at 35kV provided an important point. Moreover using parameters for the PF1000 established at 27 kV and 35 kV, additional points were taken at different voltages ranging from 13.5kV upwards to 40kV. These machines were chosen because each has a published current trace and hence the current curve computed by the model code could be fitted to the measured current trace.

Table 2. Computed values of I_{peak}, I_{pinch} , Y_n and selected parameters for a range of Focus Machines

Machine	V_o (kV)	P_o (Torr)	L_o (nH)	C_o (μF)	b (cm)	a (cm)	Z_o (cm)	I_{peak} (MA)	I_{pinch} (MA)	S	Y_n	k_{min}	I_{pinch}/I_{peak}
PF400	28	6.6	40	0.95	1.55	0.60	1.7	0.126	0.082	82	1.1×10^{06}	0.14	0.65
UNU	15	4	110	30	3.2	0.95	16	0.182	0.123	96	1.2×10^{07}	0.14	0.68
NX2 T	15	5	20	28	5	2	7	0.386	0.225	86	2.5×10^{08}	0.16	0.58
Calibration	16	5	24	308	7	4	30	0.889	0.496	99	5.6×10^{09}	0.17	0.56
NX2 T-2	12.5	10.6	19	28	3.8	1.55	4	0.357	0.211	71	2.4×10^{08}	0.16	0.59
PF1000	13.5	3.5	33	1332	8.00	5.78	60	0.924	0.507	89	9.6×10^{09}	0.17	0.55
	18	3.5	33	1332	10.67	7.70	60	1.231	0.636	89	2.9×10^{10}	0.18	0.52
	23	3.5	33	1332	13.63	9.84	60	1.574	0.766	89	6.8×10^{10}	0.19	0.49
	27	3.5	33	1332	16	11.60	60	1.847	0.862	89	1.2×10^{11}	0.19	0.47
	30	3.5	33	1332	17.77	12.80	60	2.049	0.929	89	1.6×10^{11}	0.20	0.45
	35	3.5	33	1332	20.74	15.00	60	2.399	1.037	89	2.7×10^{11}	0.20	0.43
	40	3.5	33	1332	23.70	17.10	60	2.736	1.137	89	4.1×10^{11}	0.21	0.42
Poseidon	60	3.8	18	156	9.50	6.55	30	3.200	1.260	251	3.3×10^{11}	0.20	0.39

In Table 2, corresponding to each laboratory device, the operating voltage V_o and pressure P_o are typical of the device, as is the capacitance C_o. It was found that the static inductance L_o usually needed to be adjusted from the value provided by the laboratory. This is because the value provided could be for short-circuit conditions, or an estimate including the input flanges and hence that value may not be sufficiently close to L_o. The dimensions b (outer radius), a (anode radius) and z_o (anode length) are also the typical dimensions for the specific device. The speed factor S [17] is also included. All devices except Poseidon have typical S values. Poseidon is the exceptional high speed device in this respect. The minimum pinch radius is also tabulated as $k_{min}= r_p/a$. It is noted that this parameter increases from 0.14 for the smaller machines towards 0.2 for the biggest machines. The ratio I_{pinch}/I_{peak} is also tabulated showing a trend decreasing from 0.65 for small machines to 0.4 for the biggest machines.

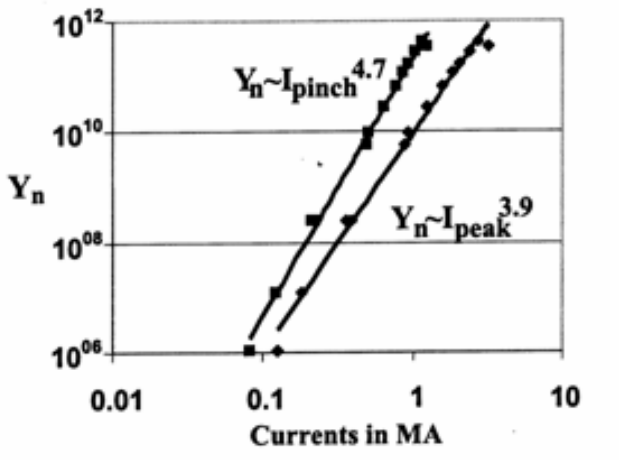

Figure 5. Computed neutron yield compiled to produce $Y_n \sim I_{peak}$ and $Y_n \sim I_{pinch}$ scaling laws

The results are the following: $Y_n=2\text{x}10^{11} I_{pinch}^{4.7}$ and $Y_n=9\text{x}10^{9} I_{peak}^{3.9}$; Y_n in units of neutrons per shot; and I_{peak} and I_{pinch} in MA.

It is felt that the scaling law with respect to I_{pinch} is rigorously obtained by these numerical experiments when compared with that obtained from measured data, which suffers from inadequacies in the measurements or assumptions of I_{pinch}.

6. Measurement of pinch current

The total current trace in a plasma focus discharge is the most commonly measured quantity. However, yield laws for plasma focus should be scaled to focus pinch current I_{pinch} rather than peak total current I_{peak}. Since the direct measurement of I_{pinch} is laborious and difficult, a reliable method for its deduction would be useful. Numerical experiments using the Lee model code can be used to determine I_{pinch} from the total current trace of a plasma focus by fitting a computed current trace to the measured current trace. The method is applied to an experiment in which both the total current trace and the plasma sheath current trace were measured. The result shows good agreement between the values of computed and measured I_{pinch}.

We now describe how we tested the validity of this method. In an experiment in Stuttgart [28,29] using the DPF78, a Rogowski coil measured the I_{total} trace, and magnetic probes measured the plasma current I_p waveform. The bank parameters were C_0=15.6 μF (nominal) and L_0=45 nH (nominal), tube parameters were b=50 mm, a=25 mm, and z_0=150 mm, and operating parameters were V_0=60 kV, and P_0=7.6 Torr deuterium. Figure 6 shows these measured I_{total} (labeled as I_{ges}) and I_p waveforms. The third trace is the difference of I_{total} and I_p.

These parameters were put into the code. The best fit for the computed I_{total} with the measured I_{total} waveform was obtained with the following: bank parameters were C_0 =17.2 μF, L_0=55 nH, and r_0=3.5 mΩ; tube parameters were b=50 mm, a=25 mm, and z_0=137 mm; and operating parameters were V_0=60 kV and P_0=7.6 Torr deuterium. Model parameters of f_m=0.06, f_c=0.57, f_{mr}=0.08, and f_{cr} =0.51 were fitted. With these parameters, the computed I_{total} trace compared well with the measured I_{total} trace, as shown in Figure 7. The computed dynamics, currents, and other properties of this plasma focus discharge were deemed to be correctly simulated.

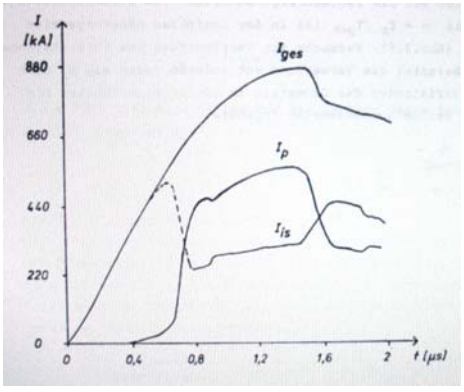

Figure 6. Experimental measurements of I_{total} (top trace) & I_p on DPF78 in Stuttgart.

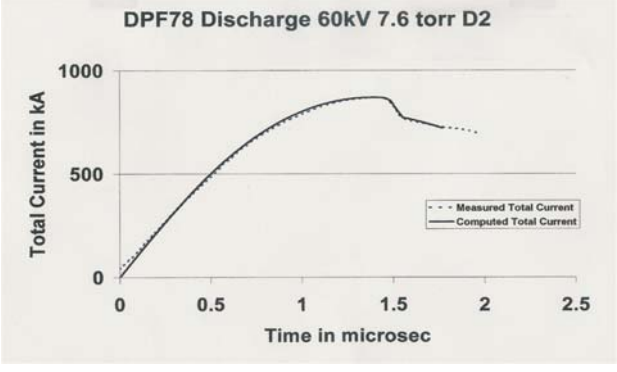

Figure 7. Fitting the computed I_{total} waveform to the measured I_{total} waveform from Figure 6

From the numerical experiments I_{pinch} was computed as 397 kA. I_{pinch} measured in the Stuttgart DPF78 experiment (Figure 6) was=381 kA. The computed I_{pinch} was 4% larger than the measured I_{pinch}. This difference was to be expected considering that the modeled f_{cr} was an average value of 0.51; while the laboratory measurement showed (Figure 8) that in the radial phase I_p/I_{total} varied from 0.63 to 0.4, and at the start of the pinch phase this ratio was 0.49 and rapidly dropping. Thus, one would expect the computed value of I_{pinch} to be somewhat higher than the measured, which turned out to be the case. Nevertheless, the difference of 4% is better than the typical error of 20% estimated for I_{pinch} measurements using magnetic probes. The numerical method proves to be a good alternative, being more accurate and convenient and only needing a commonly measured I_{total} waveform.

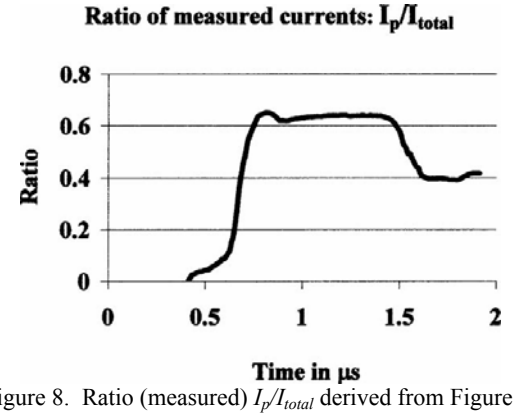

Figure 8. Ratio (measured) I_p/I_{total} derived from Figure 6.

7. Conclusion

The results of these numerical experiments indicate that corresponding to each plasma focus of capacitance C_0, there is an optimum value for L_0 below which performance in terms of I_{pinch} and Y_n does not improve. A scaling law $Y_n \sim I_{pinch}^{4.7}$ is obtained from the numerical experiments. This numerically computed scaling is more rigorous and reliable than previously obtained scaling of Y_n with loosely termed 'pinch current'. This is because we have clearly defined and rigorously computed our pinch currents. It is worth emphasizing that one of the most important ideas arising from this series of published papers is the crucial need to differentiate between the commonly-measured I_{total} and the almost-never-measured pinch current I_{pinch} in attempts to understand plasma focus processes and scaling. The Lee model code is a reliable tool to determine the pinch current.

References

[1] Lee S 1984 Radiations in Plasmas ed B McNamara (Singapore: World Scientific) pp 978–87
[2] Lee S et al 1988 Am. J. Phys. **56** 62
[3] Tou T Y, Lee S and Kwek K H 1989 IEEE Trans. Plasma Sci. **17** 311
[4] Lee S 1991 IEEE Trans. Plasma Sci. **19** 912
[5] Potter D E 1971 Phys. Fluids **14** 1911
[6] Liu M H, Feng X P, Springham S V and Lee S 1998 IEEE Trans. Plasma Sci. **26** 135–40
[7] Lee S, Lee P, Zhang G, Feng X, Gribkov V A, Liu M, Serban A and Wong T 1998 IEEE Trans. Plasma Sci. **26** 1119
[8] Bing S 2000 Plasma dynamics and x-ray emission of the plasma focus PhD Thesis NIE ICTP Open Access Archive: http://eprints.ictp.it/99/
[9] Lee S 2000/2007 http://ckplee.myplace.nie.edu.sg/plasmaphysics/
[10] Lee S 2005 ICTP Open Access Archive: http://eprints.ictp.it/85/
[11] Siahpoush V, Tafreshi M A, Sobhanian S and Khorram S 2005 Plasma Phys. Control. Fusion **47** 1065
[12] Lee S 1998 Twelve Years of UNU/ICTP PFF—A Review IC, 98 (231) Abdus Salam ICTP, Miramare, Trieste; ICTP OAA: http://eprints.ictp.it/31/
[13] L. Soto, P. Silva, J. Moreno, G. Silvester, M. Zambra, C. Pavez, L. Altamirano, H. Bruzzone, M. Barbaglia, Y. Sidelnikov & W. Kies. Brazilian J Phys 34, 1814 (2004)
[14] H.Acuna, F.Castillo, J.Herrera & A.Postal. International conf on Plasma Sci, 3-5 June 1996, conf record Pg127
[15] C.Moreno, V.Raspa, L.Sigaut & R.Vieytes, Applied Phys Letters 89(2006)
[16] D.Wong, P.Lee, T.Zhang, A.Patran, T.L.Tan, R.S.Rawat & S.Lee. Plasma Sources, Sci & Tech 16, 116 (2007)
[17] S Lee & A Serban, IEEE Trans Plasma Sci **24**, 1101-1105 (1996)
[18] Gribkov V A *et al* 2007 *J. Phys. D: Appl. Phys.* **40** 3592
[19] Lee S Radiative Dense Plasma Focus Computation Package: RADPF http://www.intimal.edu.my/school/fas/UFLF/
[20] Lee S and Saw S H 2008 Appl. Phys. Lett. **92** 021503
[21] S Lee, P Lee, S H Saw and R S Rawat. Plasma Phys. Control. Fusion **50** (2008) 065012
[22] Lee S and Saw S H Neutron scaling laws from numerical experiments J. Fusion Energy at press
[23] Lee S, Saw S H, Lee P C K, Rawat R S and Schmidt H 2008 Appl. Phys. Lett. **92** 111501
[24] J.D.Huba. 2006 Plasma Formulary pg44 http://wwwppd.nrl.navy.mil/nrlformulary/NRL_FORMULARY_07.pdf
[25] S.V.Springham, S.Lee & M.S.Rafique. Plasma Phys Control.Fusion 42, 1023 (2000)
[26] W Kies in *Laser and Plasma Technology*, Procs of Second Tropical College Ed by S Lee, B.C. Tan, C.S. Wong, A.C. Chew, K.S. Low, H. Ahmad & Y.H. Chen , World Scientific, Singapore ISBN 9971-50-767-6 (1988) p86-137
[27] H Herold in *Laser and Plasma Technology*, Procs of Third Tropical College Ed by C S Wong, S. Lee, B.C. Tan, A.C. Chew, K.S. Low & S.P. Moo, World Scientific, Singapore ISBN 981-02-0168-0 (1990) p21-45
[28] T. Oppenländer: Ph.D. Dissertation, University of Stuttgart, Germany, 1981
[29] G Decker, L Flemming, H J Kaeppeler, T Oppenlander, G Pross, P Schilling, H Schmidt, M Shakhatre and M Trunk, Plasma Physics **22**, 245-260 (1980)